NIR-emissive, singlet-oxygen-sensitizing gold tetra(thiocyano)corroles

NIR-Emissive, Singlet-Oxygen–Sensitizing Gold Tetra(thiocyano)corroles

Kasturi Sahu, Sara Angeloni, Jeanet Conradie, Marco Villa, Manisha Nayak,

Abhik Ghosh, Paola Ceroni and Sanjib Kar

Dalton Trans. 2022, 51, 13236-13245.

NIR-Emissive, Singlet-Oxygen–Sensitizing Gold Tetra(thiocyano)corroles

Kasturi Sahu,[a] Sara Angeloni,[b] Jeanet Conradie,[c, d] Marco Villa,[b] Manisha Nayak,[a] Abhik Ghosh,*[, c] Paola Ceroni,*[, b] and Sanjib Kar*[, a]

[a]*School of Chemical Sciences, National Institute of Science Education and Research (NISER), Bhubaneswar – 752050, India, and Homi Bhabha National Institute, Training School Complex, Anushakti Nagar, Mumbai, 400 094, India. E-mail: sanjib@niser.ac.in*

[b]*Department of Chemistry "G. Ciamician," University of Bologna, via Selmi 2, 40126 Bologna, Italy. E-mail: paola.ceroni@unibo.it*

[c]*Department of Chemistry, UiT – The Arctic University of Norway, N-9037 Tromsø, Norway; Email: abhik.ghosh@uit.no*

[d]*Department of Chemistry, University of the Free State, P.O. Box 339, Bloemfontein 9300, Republic of South Africa.*

Abstract: Presented herein are two fully characterized gold tetrathiocyanocorroles representing a potentially significant new class of NIR-emissive 5d-metallocorroles. The four SCN groups on the bipyrrole unit of the corrole exert a powerful electron-withdrawing effect, upshifting both the oxidation and reduction potentials by roughly half a volt relative to their unsubstituted counterparts. That said, the upshift of the LUMO is somewhat higher than that of the HOMO so these complexes also exhibit a smaller HOMO-LUMO gap, as evinced in both electrochemical measurements and Q band energies (~595 nm relative to ~571 nm for their SCN-free counterparts). The new compounds exhibit NIR phosphorescence under ambient conditions with emission maxima around 900 nm (compared with 790 nm for simple Au triarylcorroles), phosphorescence quantum yields around 0.3%, phosphorescence lifetimes around 10 μs, and singlet oxygen sensitization with a quantum yield of around 50 ± 5 % in solution, together signifying wide-ranging potential applications as triplet photosensitizers in oxygen sensing and photodynamic therapy.

KEYWORDS: Au(III)Corrole / Single-crystal XRD / DFT-calculations / phosphorescence/ singlet oxygen ($^1O_2$)

Introduction

A major facet of porphyrin or porphyrin-type molecules consists of their light absorption and emission properties. Of particular interest are 5d transition metal porphyrins, such as iridium and platinum porphyrins, which exhibit NIR phosphorescence. [1-3] Of these, Pt porphyrins have been the most widely used. In fact, they were already deployed in the previous century by Martin Gouterman as pressure-sensitive paints for the aerospace industry.[4] Today, Pt porphyrins are widely used in photomedicine as oxygen sensors as well as photosensitizers for photodynamic therapy, where their stability and biocompatibility are major considerations. [5-8] More recently, cationic Au(III) porphyrins [9] have been found to exhibit photocytotoxicity similar to that of Pt porphyrins. In recent years, the 5d metallocorroles have also emerged as a promising new class of triplet photosensitizers. Several have proved phosphorescent, including Re(V)O,[10] Os(VI)N, [11] Ir(III), [12] Pt(IV), [13] and Au(III) derivatives[14] and Au corroles[15] and to a lesser extent, ReO corroles [10] have exhibited photo-cytotoxicity against different cancer cell lines.[16-17] A key way to improve the performance of these photosensitizers is to tune the absorption of the chromophore to match the biological transparency window, in the red-NIR part of the spectrum. A promising approach has recently been outlined by Gross who found fascinating variations of photophysical properties in 2,3,17,18-tetra-Br/I/CF_3-substituted gold corroles.[18] Herein, we report a new class of Au corroles, [19-32] based on 2,3,17,18-tetrathiocyanocorrole ligands developed in one of our laboratories.[33] We accordingly describe two new complexes – 2,3,17,18-tetra(thiocyano)-10−(4−bromophenyl)−5,15−bis(4−cyanophenyl)corrolato-Au(III), **1,** and 2,3,17,18-tetrathiocyano−10−(4,7−dimethoxynaphthalen-1-yl)-5,15-bis(4-cyanophenyl) corrolato-Au(III)}, **2** (Scheme 1). Full spectroscopic characterization and one crystal structure are presented for the complexes. Excitingly, the complexes exhibit narrower electrochemical HOMO-LUMO gaps, redshifted Q bands, and strongly redshifted NIR phosphorescence relative to simple Au triarylcorroles. Like gold porphyrins, [34-36] gold corroles are also stable under physiological and photochemical conditions. In addition, there will be a great demand for the phosphorescent metalloporphyrinoid having reactive thiocyanate groups (electrophilic in nature) at the β-positions due to ease in using them as labeling reagents for various bio-analytical experiments employing Raman spectroscopy. [37]

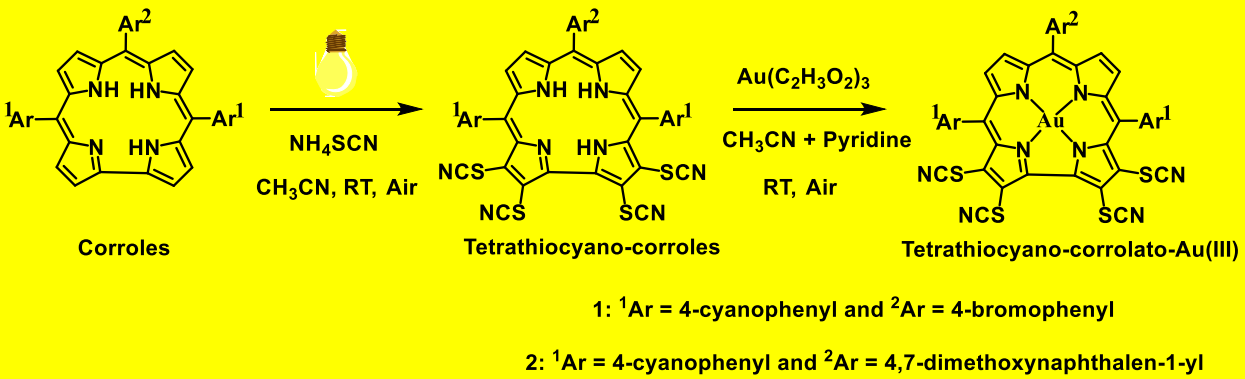

Scheme 1 Synthesis of 2,3,17,18−tetra(thiocyano)−10−(4−bromophenyl)− 5,15−bis(4−cyano−phenyl) corrolato-Au(III)}, **1** and 2,3,17,18-tetrathiocyano−10−(4,7−dimethoxynaphthalen-1-yl)-5,15-bis(4-cyanophenyl) corrolato-Au(III)}, **2**.

RESULTS AND DISCUSSION

Synthesis and characterization

FB 2,3,17,18-tetrathiocyano corroles (FB = free base) were prepared by following an earlier literature method developed by us.[33] Gold metallation was performed into the FB 2,3,17,18-tetrathiocyano corrole cavity by using gold acetate as a metal precursor in an acetonitrile and pyridine mixture at RT {RT= room temperature) in the aerial condition.[21] The composition and purity of the 2,3,17,18-tetra(thiocyano)corrolato-Au(III) complexes (**1**−**2**) were established by a series of analytical techniques, i.e. CHN analyses, UV/Vis, FTIR spectroscopy, ESI-HRMS, NMR, and single-crystal XRD analysis (Figs S1-S9, see ESI†). The diamagnetic nature of the 2,3,17,18-tetra(thiocyano)corrolato-Au(III) complexes (**1**−**2**) is evident from their sharp peaks with normal chemical shifts at the expected regions. The ^{1}H NMR spectrum of both **1** and **2** exhibits intense peaks in the region δ, ~ 8.50–7.86 ppm and δ, ~ 8.49–6.40 ppm respectively. In the case of complex **2**, two sets of sharp singlets appeared at 4.22 and 3.24 ppm corresponding to two sets of methoxy protons. The FT-IR spectra (as KBr pellets) of **1-2** exhibited strong S-CN stretching vibration at 2164, and 2157 cm^{-1}, respectively (Figs S5-S6, see ESI†).

Crystal Structure

The crystal system of 2,3,17,18-tetrathiocyano−10−(4,7−dimethoxynaphthalen-1-yl)-5,15-bis(4-cyanophenyl) corrolato-Au(III)}, **2** is orthorhombic and the unit cell has sixteen molecules of **2** (Fig. 1). Important crystallographic parameters for **2** are summarized in Table 1. Key features of the structure are similar to those observed in previously obtained structures for Au corroles. The bite angles of N1-Au-N2, N2-Au-N3, N3-Au-N4, and N4-Au-N1 are 92.03°, 95.08°, 91.65°, and 81.20°, respectively and matches well with the earlier reported Au(III) corroles.[25] Thus, the Au-N bond distances are 1.95 ± 0.01 Å and are typical for Au(III) corroles. Also, **2** exhibits a longer pyrrole-pyrrole linkage, i.e., a C1-C19 bond length of 1.452 Å. The analogous bond distances in earlier reported corrolato-Au(III) derivatives are generally in the range of 1.40-1.42 Å.[20, 29] Along with a slightly higher degree of bond length alternation in the corrole skeleton, this geometrical peculiarity suggests reduced aromatic character in **2**, as a result of thiocyanation. In other respects, the planar coordination geometry of the Au(III) center (ionic radiuss 0.85 Å) is similar to that of other Au corroles,[20] but tighter than that of porphyrins.

Table 1 Crystallographic Data for **2**.

compound code	**2**
chemical formula	$C_{49}\ H_{23}\ Au\ N_{10}\ O_2\ S_4$
formula mass	1108.98
crystal system	Orthorhombic
crystal size (mm)	0.13×0.12×0.10
space group	*F dd2*
Radiation	Cu *K*α
a(Å)	52.0552 (6)
b(Å)	51.4324 (5)
c(Å)	7.14602 (8)
α (deg)	90
β (deg)	90
γ (deg)	90
V(Å^3)	19132.2(4)
Z	16
T(K)	100
D_{calcd} (g cm^{-3})	1.540
measured reflections	33394
e data (R_{int})	7692 (0.085)
parameters	573
restraints	172
μ (mm^{-1})	7.82
2θ range (deg)	3.78-77.12
R1 (*I*>2σ(*I*))	0.073
WR2 (all data)	0.168
S (GooF) all data	1.04
$\Delta\rho_{max}$, $\Delta\rho_{min}$ (e Å^{-3})	1.87, −1.55

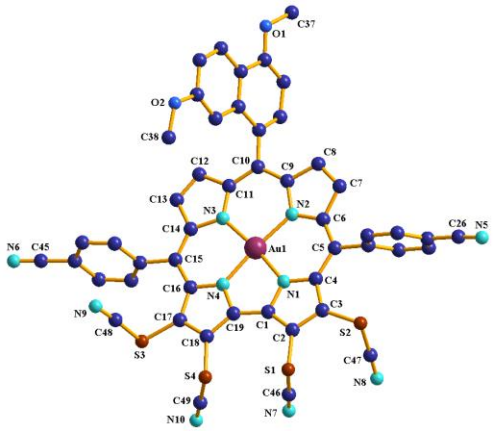

Fig. 1 Single-crystal X-ray structure of **2**. Hydrogen atoms are omitted for clarity.

Unlike Cu corroles,[38] which are invariably saddled, **2**, like other Au corroles, is essentially planar with C2-C1-C19-C18 and C8-C9-C11-C12 dihedrals around only 6.7° and 14.7°. The saddling of Cu corroles reflects ligand noninnocence, as noted elsewhere, a scenario that does not apply to Au corroles.[22,39]

Electrochemistry

To understand the redox properties of **1** and **2**, the cyclic voltammetric and differential pulse voltammetric measurements were performed in dichloromethane (Fig. 2 and Table 2). Tetraethyl ammonium perchlorate (TEAP, 0.1 M) was used as a supporting electrolyte and Ag/AgCl electrode was used as a reference electrode.

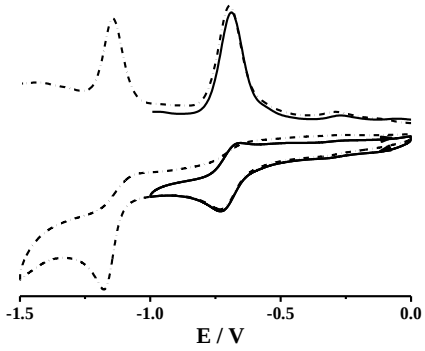

Fig. 2 Cyclic voltammogram (black solid line) and differential pulse voltammogram (black dash-dot line) of **2** in CH_2Cl_2 under a nitrogen atmosphere. The potentials are *vs.* Ag/AgCl.

Table 2 UV–Vis and electrochemical data of compounds **1**, **2**, **1a** (*β*-unsubstituted corrolato-Au(III) analogue of compound **1**), and **2a**[25] (*β*-unsubstituted corrolato-Au(III) analogue of compound **2**) in dichloromethane.

Compound	UV–vis. Data [a]	Electrochemical data [a,b]	
	λ_{max} / nm (ε / $M^{-1}cm^{-1}$)	Oxidation	Reduction
		E^0, V (ΔE_p, mV)	E^0, V (ΔE_p, mV)
1	403 (44000), 421 (40800), 537 (12200), 554 (17300), 578 (37700), 595 (45000)	+1.30	-0.66 (90), -1.13
2	403 (45800), 422 (41000), 537 (13800), 554 (19000), 580 (43000), 596 (42100)	+1.28	-0.69 (90), -1.14
1a[c]	422 (133000), 498 (4800), 534 (11400), 570 (51000)	+0.78 (80), +1.15 (80)	-1.28 (80)
2a[25]	423 (142000), 494 (3700), 533 (9300), 572 (37000)	+0.88 (70), +1.25 (80)	-1.32 (80), -1.67 (80)

[a] In dichloromethane.

[b] The potentials are vs. Ag/AgCl

[c] Unpublished data

The tetra(thiocyano)corrolato-Au(III) derivatives, **1** and **2** exhibited one reversible and one irreversible reductive couples. The 1st reversible reductive couple is observed at -0.66 V and the 2nd irreversible reduction couple is observed at -1.13V *vs.* Ag/AgCl for complex **1**. This compound also exhibited one oxidative couple at 1.30 V. The 1st reversible reductive couple is observed at -0.69 V and the 2nd irreversible reduction couple is observed at -1.14V for complex **2**. This compound also exhibited one oxidative couple at 1.28 V. The separation between 1st oxidative couple and the 1st reductive couple is ~2.0 V in both of these complexes. The above redox potentials are dramatically upshifted, by roughly half a volt, relative to those of the non-thiocyanted complexes.[25] These upshifts are consistent with the Hammett σ_p and σ_m of the SCN

groups, which are about the same as those of CN and CF_3 groups. The σ_p and σ_m values for SCN group are 0.52 and 0.51 respectively. The corresponding values for CN group are 0.66 and 0.56 respectively. The values for CF_3 group are 0.54 and 0.43 respectively.[40] Interestingly, thiocyano groups have been much less frequently deployed as electron-withdrawing substituents than CN and CF_3, indicating that they may deserve broader exploration. Careful examination of Table 2 shows that tetrathiocyano-substitution upshifts the reduction potentials somewhat more than the oxidation potentials, resulting in a smaller electrochemical HOMO-LUMO gap for **1** and **2** (about 1.95-2.0 V) than for their non-thiocyanated counterparts.

Photophysical properties

The UV-Vis spectra of tetra(thiocyano)corrolato-Au(III) derivatives **1-2** (Fig. 3) are significantly modified in comparison to the *β*-unsubstituted corrolato-Au(III) derivatives (see Fig. S2 for a direct comparison in dichloromethane solution).[25] The Soret band is split into at least two distinct bands and so also the Q bands. The tail of Q bands reached up to 650 nm. This kind of absorption profile is clearly absent in the case of *β*-unsubstituted corrolato-Au(III) derivatives with similar corrole back bone.[25] The 2,3,17,18-*tetra*-SCN-substitution in corrole periphery thus can alter the HOMO and LUMO energy spacing and thus can essentially change the transition energies for Q bands. The Q absorption bands of these *β*-substituted corrolato-Au(III) derivatives are peaked in the red spectral region, a suitable window for PDT and other bioimaging applications, which are not possible in the frequently encountered *β*-unsubstituted corrolato metal complexes. Tetrathiocyanation has a dramatic impact on the UV-vis spectra of the Au corroles. The most notable effect is on the extinction coefficient of the Soret band, which is dramatically weaker in the tetrathiocyano complexes. By comparison, the Q band intensities are much less affected. These differences translate to nearly equal intensities of both the Soret and Q bands for **1** and **2**, an uncommon occurrence for simple porphyrins and corroles, which follow the Gouterman four-orbital model. A second notable effect of tetrathiocyanation is a redshift of the lowest-energy Q band by about 25 nm, qualitatively consistent with a lowering of the electrochemical HOMO-LUMO gap, as mentioned above.

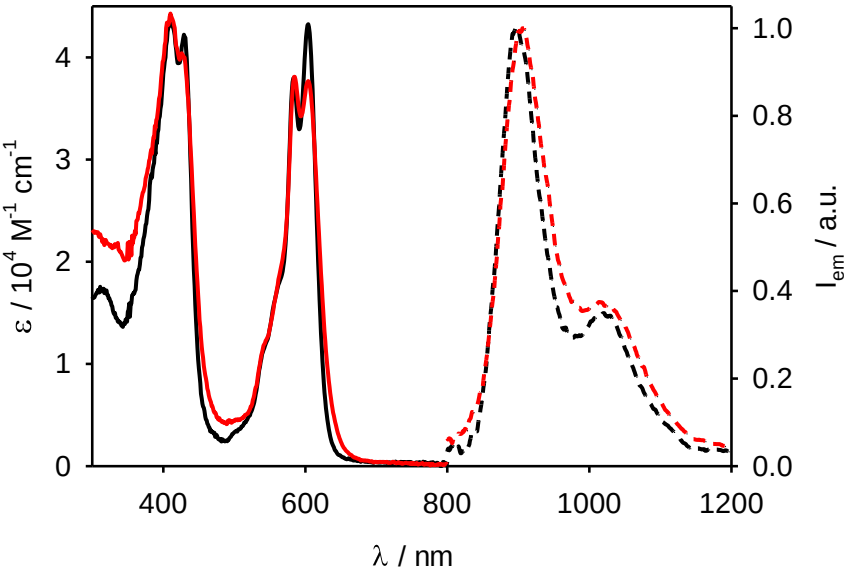

Fig. 3 Absorption (solid lines) and normalized phosphorescence spectra (dashed lines) of compounds **1** (black lines) and **2** (red lines) in degassed toluene solution at 298 K. λ_{exc}=410nm.

Compounds **1** and **2** exhibit an emission band peaked at ca. 900 nm (Fig. 3) in degassed toluene solution (λ_{exc}=410nm). The excitation spectra registered at the emission maximum closely match the corresponding absorption spectra (Fig. S3), demonstrating that the Au(III) corrolato complexes are responsible for this near infrared emission. The emission intensity decays can be fitted by mono exponential curves with lifetimes of 9.98 and 10.18 μs for complexes **1** and **2** respectively (Fig. S4), demonstrating that the observed radiative decay is phosphorescence. As previously reported in the literature,[28] we observe a strong solvent effect on the emission quantum yield: indeed, no emission could be detected for degassed chloroform solutions of **1** and **2**. Compounds **1** and **2** can efficiently sensitize the singlet oxygen population (Table 3), as demonstrated by the characteristic phosphorescence of singlet oxygen at 1270 nm upon selective excitation of Au(III) corrolato complexes at 615 nm in chloroform solution.

Table 3. Photophysical data of compounds **1** and **2**. The conditions are toluene solution at 298 K, unless otherwise noted.

	λ_{abs} / nm	ε /10^4 M^{-1} cm^{-1}	λ_{em} / nm	Φ_{em} [a]	τ / μs[a]	Φ ($^1O_2$) [b]
1	409, 603	4.33, 4.32	898	0.28%	9.98	57%
2	409, 604	4.42, 3.76	905	0.30%	10.18	46%

[a]Emission quantum yields and lifetime measured in degassed toluene solution. [b]Quantum yield of singlet oxygen ($^1O_2$) production in chloroform solution upon excitation at 615 nm.

DFT and TDDFT calculations

Scalar-relativistic (ZORA) DFT and TDDFT calculations provide a coherent rationale for many of the experimental observations outlined above. The experimentally studied compounds were modeled with Au[TPC] and Au[TPC(SCN)$_4$]. The calculations were carried out with three different exchange-correlation functionals (OLYP, B3LYP, and B3LYP*) and all-electron ZORA STO-TZ2P basis sets. The optimized geometries of Au[TPC] and Au[TPC(SCN)$_4$] (Fig. 4) proved nicely consistent with experimental results on simple Au-triarylcorroles and **2**. Thus, the calculated Au-N distances were in essentially perfect agreement with experiment. The calculations also confirmed the essential planarity or very mild saddling of the corrole macrocycle. Interestingly, examination of the optimized geometries revealed an interesting larger skeletal bond distance alternations for Au[TPC(SCN)$_4$] than for Au[TPC], which appear to be consistent with the aforementioned crystallographic results. Also, Au[TPC(SCN)$_4$] exhibits a longer pyrrole-pyrrole linkage than Au[TPC], indicating reduced aromatic character upon thiocyanation.

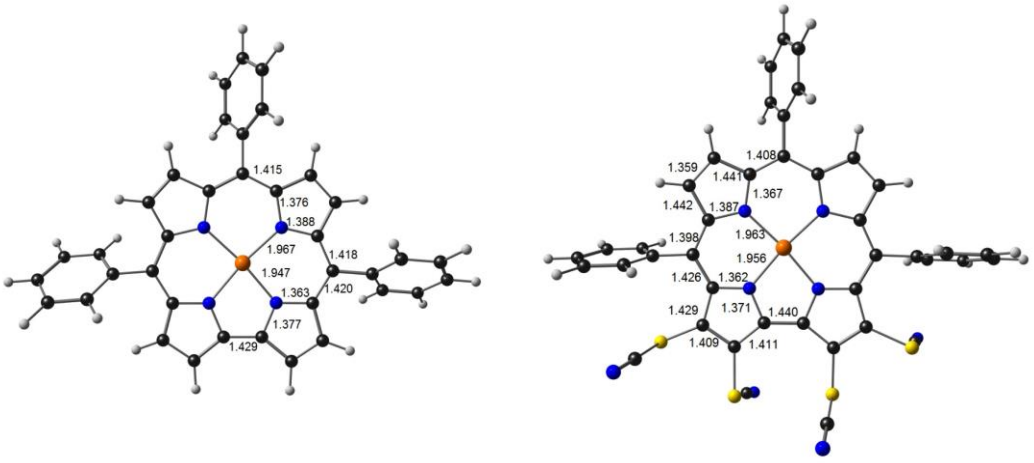

Fig. 4 Selected distances (Å) in the optimized geometries of Au[TPC] and Au[TPC(SCN)$_4$].

Table 4 presents DFT calculations of the gas-phase IPs and EAs (both vertical and adiabatic) of Au[TPC] and Au[TPC(SCN)$_4$]. Based on earlier simulations of photoelectron spectra and redox potentials,[61-69] these values are thought to be semi-quantitatively accurate. This conclusion is bolstered by the high level of consistency among the three functionals used, even though we believe the B3LYP* values as the most accurate. The calculations confirm the very strong electron-withdrawing effect of the thiocyano groups. Tetrathiocyanation upshifts the IP and EA of Au[TPC] by 0.9 and 1.3 eV, respectively. The higher substituent effects (relative to what is observed electrochemically) are typical of gas-phase results. The spin density profiles of the ionized states of Au[TPC(SCN)$_4$], however, are very similar to those of unsubstituted Au[TPC], indicating that the qualitative shapes of the redox-active MOs are not affected by the thiocyano groups.

Table 4 Calculated IPs and EAs (eV).

Compound	Functional	Adiabatic		Vertical	
		IP	EA	IP	EA
Au[TPC]	OLYP	5.97	1.32	6.01	1.14
	B3LYP	6.04	1.39	6.11	1.28
	B3LYP*	6.04	1.38	6.11	1.27
Au[TPC(SCN)$_4$]	OLYP	6.43	2.46	6.80	2.34
	B3LYP	6.93	2.68	7.11	2.61
	B3LYP*	6.94	2.67	7.14	2.60

Fig. 5 presents the B3LYP* simulated TDDFT spectra of Au[TPC] and Au[TPC(SCN)$_4$] in dichloromethane using the COSMO solvation model.[41,42] The corresponding data are presented in Table 5. An MO energy level diagram and the relevant MOs are depicted in Fig. 6 and Fig. 7, respectively. Observe that the calculations qualitatively reproduce the two spectral features emphasized above, namely a sharp reduction in the Soret band intensity and a redshift of the lowest-energy Q band upon thiocyanation. Both these features appear to be related to the reduction of macrocycle aromaticity upon thiocyanation. The Kohn-Sham orbital energies are also qualitatively consistent with the dramatic upshifts in both oxidation and reduction potential upon thiocyanation. Also consistent with the experiment is the greater downshift of the LUMO energy, compared to the HOMO, which results in a narrowing of the HOMO-LUMO gap and a widening of the LUMO/LUMO+1 gap (the so-called DLUMO, according to Michl's perimeter model.[70] The latter also provides an alternative explanation of the relative intensity of the Q band. Thiocyanation also significantly upshifts the Au 5d$_{x2-y2}$ orbital, the LUMO +2, but to a lesser degree than the LUMO.[43]

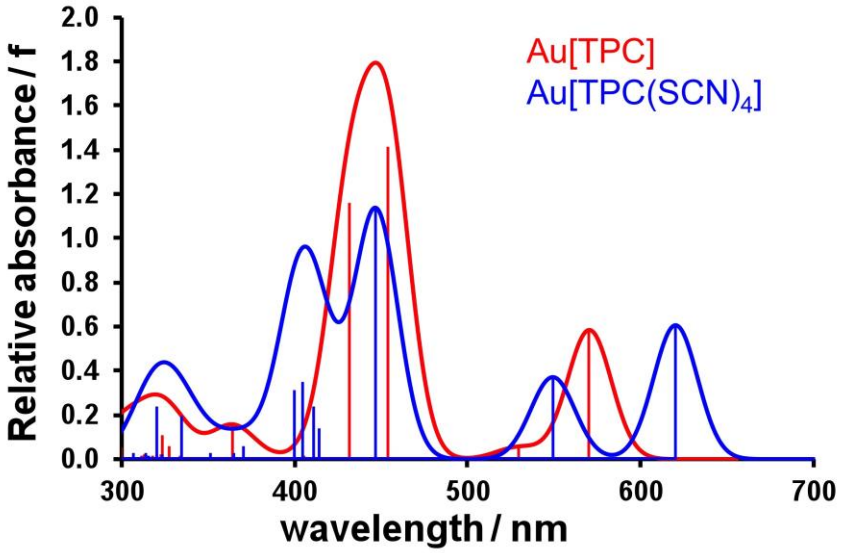

Fig. 5 Simulated TD-B3LYP*-COSMO optical spectra Au[TPC] and Au[TPC(SCN)$_4$] in dichloromethane. The vertical lines represent calculated transitions which have then been broadened with Gaussians to generate the simulated spectra.

Table 5 B3LYP*/ZORA-STO-TZ2P TDDFT results, including transition energies (*E*) and wavelengths (λ), oscillator strengths (*f*), MO compositions, and excited-state irreps.

compound	peak	*E* (eV)	*l* (nm)	*f*	weight	from	to	C_2 irrep
Au[TPC]	Q	2.17	570.3	0.58	92%	HOMO	LUMO	B
					7%	HOMO-1	LUMO+1	B
		2.34	529.4	0.05	71%	HOMO-1	LUMO	A
					28%	HOMO	LUMO+1	A
	Soret	2.73	454.0	1.42	69%	HOMO	LUMO+1	A
					27%	HOMO-1	LUMO	A
		2.87	431.8	1.16	91%	HOMO-1	LUMO+1	B
					6%	HOMO	LUMO	B
Au[TPC(SCN)$_4$]	Q	2.00	620.4	0.61	96%	HOMO	LUMO	B
					3%	HOMO-1	LUMO+1	B
		2.26	549.3	0.37	89%	HOMO-1	LUMO	A
					10%	HOMO	LUMO+1	A
	Soret	2.77	446.9	1.13	83%	HOMO	LUMO+1	A
					8%	HOMO-1	LUMO	A
					6%	HOMO-3	LUMO	A
		2.99	414.0	0.14	78%	HOMO-1	LUMO+2	B
					11%	HOMO-1	LUMO+1	B
					9%	HOMO-2	LUMO	B
		3.02	410.9	0.24	58%	HOMO-2	LUMO	B
					21%	HOMO-1	LUMO+1	B
					19%	HOMO-1	LUMO+2	B
		3.06	404.7	0.35	60%	HOMO-1	LUMO+1	B
					30%	HOMO-2	LUMO	B
		3.10	399.7	0.31	92%	HOMO-3	LUMO	A

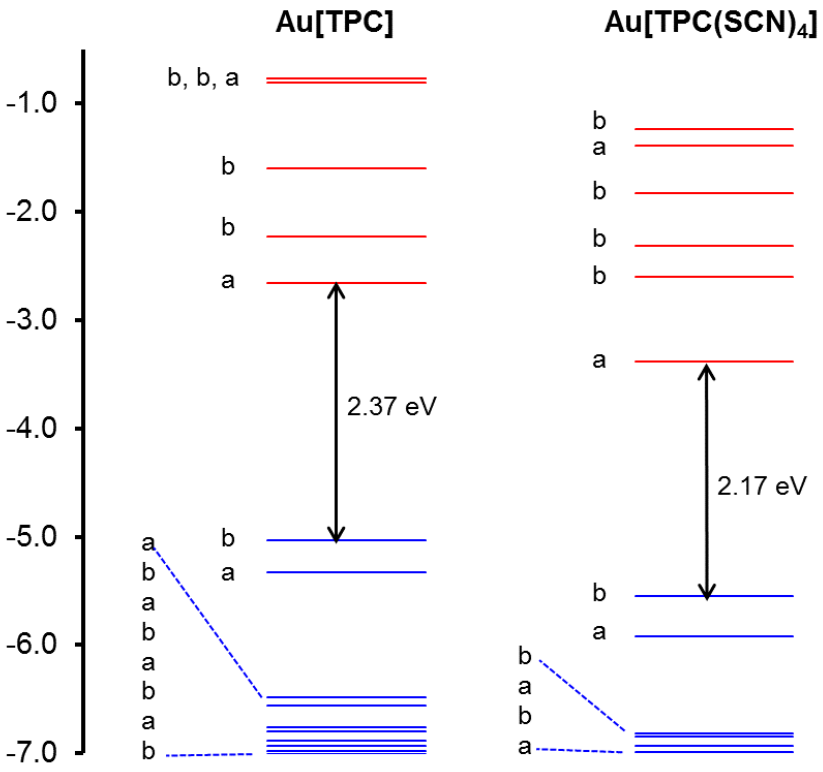

Fig. 6 B3LYP*-D3/STO-TZ2P Kohn-Sham MO energy (eV) level diagram of Au[TPC] and Au[TPC(SCN)$_4$], in dichloromethane modelled with COSMO. Selected frontier MOs, along with their irreps and orbital energies shown. Unoccupied MOs are shown in red and occupied MOs in blue.

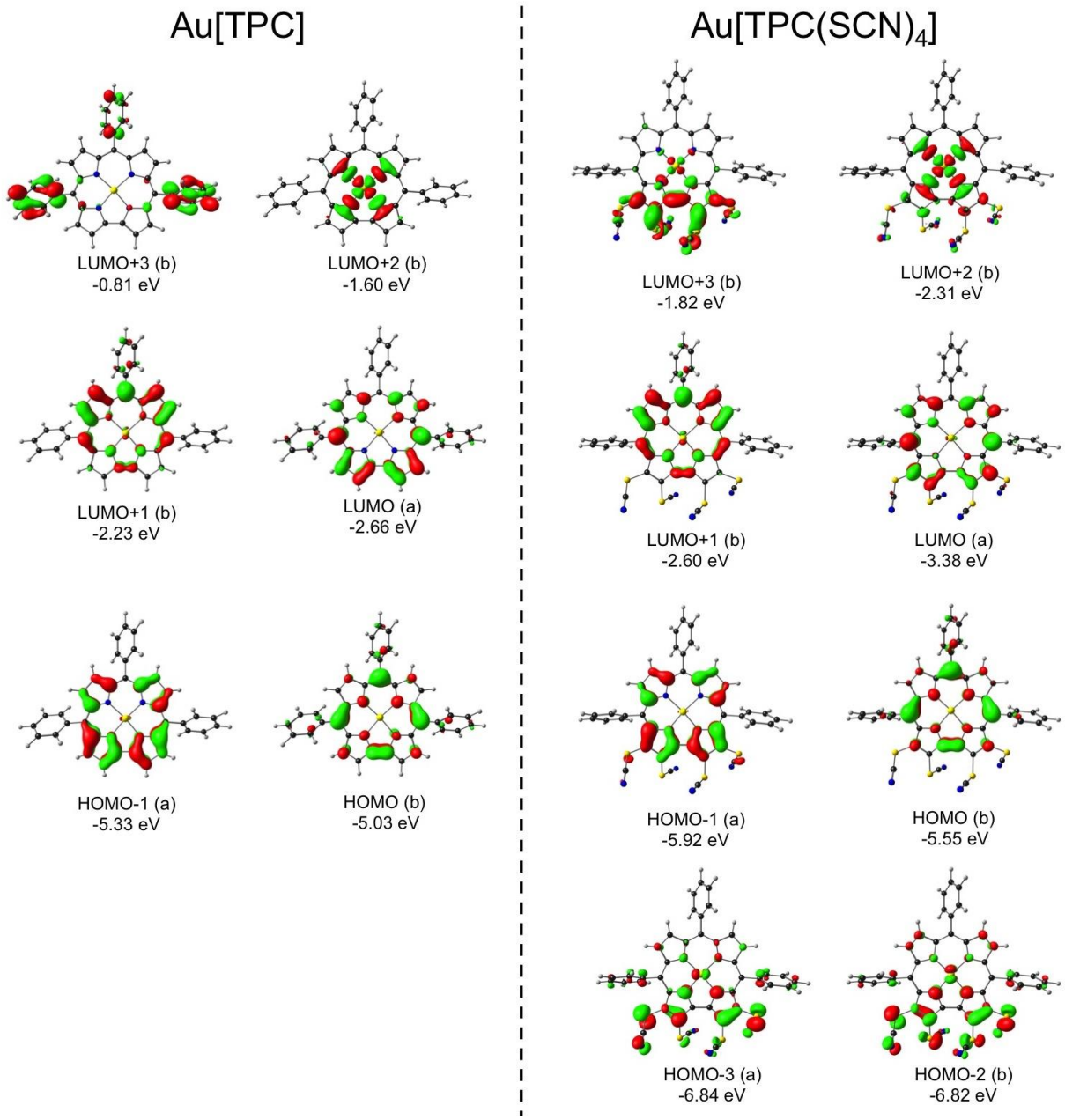

Fig. 7 Selected frontier MOs, along with their irreps and orbital energies, of Au[TPC] and Au[TPC(SCN)$_4$].

Conclusions

We have described the synthesis and full spectroscopic characterization of two gold 2,3,17,18-tetra(thiocyano)corrole complexes, which represent a new class of peripherally functionalized 5d metallocorroles. An X-ray structure revealed a near-planar corrole macrocycle with relatively normal Au-N bond distances of 1.95 ± 0.01 Å. The electronic properties of the compounds, on the other hand, turned out to be dramatically different, relative to simple Au triarylcorroles. Thus, both the oxidation and reduction potentials of the new complexes were found to be about half a volt upshifted relative to their *β*-unsubstituted analogs. The new compounds were also found to exhibit a narrower electrochemical HOMO-LUMO gap, which is also echoed in a redshifted Q band at 595-596 nm, compared to 570-572 nm for their unsubstituted counterparts. The compounds also appear to exhibit reduced aromaticity, as evidenced by increased skeletal bond length alternations and relatively weak Soret bands with intensities, surprisingly, approximately the same as those of Q bands. By comparison, the Q band intensities are much less affected. The redshifted Q band maxima in turn are reflected in a redshifted phosphorescence emission maximum around 900 nm in degassed toluene, the phosphorescence quantum yield and lifetime being 0.3% and 10 μs, respectively. The new compounds **1** and **2** were also found to efficiently sensitize singlet oxygen formation in chloroform with quantum yields of 57% and 46%, respectively. The compounds accordingly appear promising for potential applications in oxygen sensing, photodynamic therapy, and other applications in photo-medicine.

EXPERIMENTAL SECTION

Materials

The precursor's pyrrole, *p*-chloranil, aldehydes were purchased from Aldrich, USA and gold acetate (99.99%) from Alfa Aesar. NH_4SCN (>98.5% purity), pyridine, acetonitrile (HPLC) was purchased from Merck chemicals. Other chemicals were of reagent grade. Hexane, CH_2Cl_2, CH_3CN were distilled from KOH and CaH_2 respectively. For spectroscopy studies, HPLC grade solvents were used. For the synthesis of FB corroles, a protocol developed by Gryko et al. was used.[44] The synthetic methodologies and full spectroscopic characterization of free base corroles: 2,3,17,18-tetra(thiocyano)−10−(4−bromophenyl)−5,15−bis(4−cyanophenyl) corrole and 2,3,17,18-tetrathiocyano−10−(4,7−dimethoxynaphthalen-1-yl)-5,15-bis(4-cyanophenyl) corrole were reported earlier by us. [33]

Physical Measurements

The elemental analyses were carried out with a Euro EA elemental analyser. UV−Vis spectral studies were performed on a Perkin−Elmer LAMBDA-750 spectrophotometer. Emission spectra were performed on an Edinburgh FLS920 spectrofluorometer equipped with a Ge-detector for emission in the NIR spectral region, using optical cell of 1 cm path length. Luminescence lifetime were recorded with an Edinburgh FS5 equipped with a PMT980. Emission quantum yields were measured following Demas and Crosby method[45] (standard used: HITCI (1,1′,3,3,3′,3′-hexamethyl-indotricarbocyanine iodide) in EtOH $\Phi = 0.30$).[46] The singlet oxygen generation [24] from the chloroform solutions was measured using a chloroform solution of 5,10,15,20-Tetraphenyl-21H,23H-porphine (TPP) as the reference with a singlet oxygen production yield of 55%.[47] The three solutions have been excited in an isosbestic point (615 nm) and the singlet oxygen emissions were detected in a range from 1220 to 1330 nm and compared. FT−IR spectra were recorded on a Perkin−Elmer spectrophotometer with samples prepared as KBr pellets. The NMR measurements were carried out using a Bruker 400 MHz NMR spectrometer. Chemical shifts are expressed in parts per million (ppm) relative to residual chloroform (δ= 7.26). Electrospray mass spectra were recorded on a Bruker Micro TOF─QII mass spectrometer. Cyclic voltammetry measurements were carried out using a CS350 electrochemical test system (China). A glassy carbon working electrode, a platinum wire as an auxiliary electrode, and an Ag-AgCl reference electrode were used in a three-electrode configuration. Tetrabutylammonium perchlorate (TBAP)

was the supporting electrolyte (0.1 M), and the concentration of the solution was 10^{-3} M with respect to the complex. The half-wave potential E^0_{298} was set equal to 0.5 (E_{pa} + E_{pc}), where E_{pa} and E_{pc} are anodic and cathodic cyclic voltammetric peak potentials, respectively. The scan rate used was 100 mV s^{-1}.

Crystal Structure Determination: Single crystals of **2** were grown from the solution of **2** in dichloromethane-hexane mixture (1:1), followed by slow evaporation under atmospheric conditions. ORTEP diagram of **2** is shown in Fig. S1 (hydrogen atoms are omitted for clarity). Ellipsoids are drawn at 50% probability. The crystal data of **2** were collected on a Rigaku Oxford diffractometer (Cu *K*α radiation) at 100 K. Selected data collection parameters and other crystallographic results are summarized in Table S1. All data were corrected for Lorentz polarization and absorption effects. The program package SHELXTL[48] was used for structure solution and full matrix least squares refinement on F^2. Hydrogen atoms were included in the refinement using the riding model. Contributions of H atoms for the water molecules were included but were not fixed. Disordered solvent molecules were taken out using SQUEEZE command in PLATON.[49] Single crystals of **2** had poor diffraction quality. From such low-quality crystals, we have not obtained the good quality residual density map, normal probability plot, and the F_{obs} vs F_{calc} plot. CCDC 2122129 contains the supporting crystallographic data for **2**. These data can be obtained free of charge via www.ccdc.cam.ac.uk/data_ request/cif.

Synthesis of 2,3,17,18-tetra(thiocyano)−10−(4−bromophenyl)−5,15−bis(4−cyanophenyl) corrolato-Au(III)}, 1

25mg (0.028mmol) of 2,3,17,18-tetra(thiocyano)−10−(4−bromophenyl)−5,15−bis(4−cyanophenyl) corrole was dissolved in 5ml of acetonitrile, and then 60mg (0.16 mmol) of gold acetate was added to it followed by 12ml of pyridine. The reaction mixture was stirred at room temperature for 1 h in air. After that, the solvent was evaporated, and the brown color crude product was subjected to column chromatography using a silica gel (100–200 mesh) column. The desired product (reddish blue) was eluted by using a mixture of 93% DCM and 7% acetonitrile. The final form of the compound was obtained as pinkish crystalline materials

For 2,3,17,18-tetra(thiocyano)−10−(4−bromophenyl)−5,15−bis(4−cyanophenyl) corrolato-Au(III)}, 1

Yield: 33% (10 mg). Anal. Calcd for $C_{43}H_{16}AuBrN_{10}S_4$ (**2**): C, 47.92; H, 1.50; N, 13.00. Found: C, 47.81; H, 1.42; N, 13.16. $\lambda_{max/nm}$ (ε/$M^{-1}cm^{-1}$) in CH_2Cl_2: 403 (44014), 421 (40845), 537 (12233), 554 (17348), 578 (37719), 595 (44950) (Fig. S2). ^{1}H NMR (400 MHz, Chloroform-*d*) δ 8.50 (d, *J* = 5.1 Hz, 2H), 8.43 (d, *J* = 5.1 Hz, 2H), 8.23 – 8.08 (m, 8H), 7.93 (d, *J* = 8.0 Hz, 2H), 7.86 (d, *J* = 8.1 Hz, 2H) (Fig. S9). HRMS (ESI) *m/z*: $[2+Na]^+$ Calcd for $C_{43}H_{16}AuBrN_{10}S_4Na$ 1098.9183; Found 1098.7538 (Fig. S7).

Synthesis of 2,3,17,18-tetrathiocyano−10−(4,7−dimethoxynaphthalen-1-yl)-5,15-bis(4-cyanophenyl) corrolato-Au(III)}, 2

25mg (0.027 mmol) of 2,3,17,18-tetrathiocyano−10−(4,7−dimethoxynaphthalen-1-yl)-5,15-bis(4-cyanophenyl) corrole was dissolved in 4 ml of acetonitrile, and then 60 mg of gold acetate (0.16mmol) was added to it followed by 12ml of pyridine. The reaction mixture was stirred at room temperature for 1h in the air. After that, the solvent was evaporated, and the brown color crude product was subjected to column chromatography using a silica gel (100–200 mesh) column. The desired product (reddish pink) was eluted using a mixture of 95% dichloromethane and 5% acetonitrile. The final form of the compound was obtained as pinkish crystalline materials.

For 2,3,17,18-tetrathiocyano−10−(4,7−dimethoxynaphthalen-1-yl)-5,15-bis(4-cyanophenyl) corrolato-Au(III)}, 2

Yield: 34% (10 mg). Anal. Calcd for $C_{49}H_{23}AuN_{10}O_2S_4$ (**1**): C, 53.07; H, 2.09; N, 12.63. Found: C, 53.17; H, 2.16; N, 12.78. $\lambda_{max/nm}$ (ε / $M^{-1}cm^{-1}$) in CH_2Cl_2: 403 (45799), 422 (41020), 537 (13811), 554 (18997), 580 (43006), 596 (42058) (Fig. S2). ^{1}H NMR (400 MHz, Chloroform-*d*) δ 8.49 (d, *J* = 9.3 Hz, 1H), 8.31 – 8.23 (m, 4H), 8.18 (dd, *J* = 15.4, 7.2 Hz, 4H), 8.10 (d, *J* = 8.3 Hz, 4H), 7.83 (d, *J* = 7.8 Hz, 1H), 7.21 (d, *J* = 2.4 Hz, 1H), 7.05 (d, *J* = 8.0 Hz, 1H), 6.40 (d, *J* = 2.7 Hz, 1H), 4.22 (s, 3H), 3.24 (s, 3H) (Fig. S10). HRMS (ESI) *m/z*: [**1**+Na]$^+$ Calcd for $C_{49}H_{23}AuN_{10}O_2S_4Na$ 1131.0446; Found 1131.0570 (Fig. S8).

Computational Methodology:

All calculations employed scalar relativistic DFT, the ZPRA Hamiltonian, well-tested exchange-correlation functionals (OLYP,[50,51] B3LYP,[51,52] and B3LYP*,[53] all-electron ZORA STO-TZ2P basis sets, tight critetia for SCF and geometry optimization cycles, fine integration grids, and, unless otherwise mentioned the COSMO aolvation model and dichloromethane as solvent, all as implemented in ADF-2019.[54-60] The solvent was omitted only in calculations of IPs[61-66] and EAs.[67-69] Because of the conformational flexibility of the SCN groups, great care was exercised to correctly identify the global minima of the molecules studied.

ASSOCIATED CONTENT

† Electronic Supplementary Information (ESI) available:

Crystallographic data, UV-Vis, FT-IR, ESI-MS, ^{1}H-NMR data, and Optimized Cartesian coordinates (Å). Crystallographic data for compound **2** (CIF). CCDC 2122129 contains the supplementary crystallographic data for **2**. These data can be obtained free of charge via www.ccdc.cam.ac.uk/data_request/cif.

AUTHOR INFORMATION

Corresponding Authors

E-mail: sanjib@niser.ac.in, paola.ceroni@unibo.it, abhik.ghosh@uit.no

ORCID

Sanjib Kar: 0000-0002-0203-8884

Paola Ceroni: 0000-0001-8916-1473

Abhik Ghosh − 0000-0003-1161-6364

Villa: 0000-0002-1792-159X

Sara Angeloni: 0000-0003-4957-9642

Jeanet Conradie: 0000-0002-8120-6830

Conflicts of interest

There are no conflicts of interest to declare.

ACKNOWLEDGEMENTS

We gratefully acknowledge financial support from the Department of Atomic Energy (India), the University of Bologna, the Research Council of Norway (grant no. 324139 to AG), and the South African National Research Foundation (grant nos. 129270 and 132504 to JC). The authors thankfully acknowledge NISER-Bhubaneswar for providing infrastructure. K.S thanks CSIR India for a research fellowship.

REFERENCES

1. A. P. Savitsky, A. V. Savitskaja, E. A. Lukyanets, S. N. Dashkevich and E. A. Makarova, 1997.
2. F. Niedermair, S. M. Borisov, G. Zenkl, O. T. Hofmann, H. r. Weber, R. Saf and I. Klimant, , *Inorg. Chem.*, 2010, **49**, 9333-9342.
3. K. Koren, R. I. Dmitriev, S. M. Borisov, D. B. Papkovsky and I. Klimant, *ChemBioChem*, 2012, **13**, 1184-1190.
4. A. Ghosh, *Angew. Chem., Int. Ed.*, 2021, **60**, 9760-9770.
5. (a) (a) X.-d. Wang and O. S. Wolfbeis, *Chemical Society Reviews*, 2014, **43**, 3666-3761.; (b)A. Garai, M. Villa, M. Marchini, S. K. Patra, T. Pain, S. Mondal, P. Ceroni and S. Kar, *Eur. J. Inorg. Chem.*, 2021, **2021**, 4089-4095.
6. R. K. Pandey, T. J. Dougherty and D. Kessel, *Handbook of photodynamic therapy: updates on recent applications of porphyrin-based compounds*, World Scientific, 2016.
7. R. Bonnett and M. Berenbaum, *Photosensitizing compounds: their chemistry, biology and clinical use*, 1989, **146**, 40-53.
8. P. M. Pereira, Tomé, J.P. and Fernandes, R., 2016, vol. 39, pp. 127-169.
9. I. Toubia, C. Nguyen, S. Diring, L. M. Ali, L. Larue, R. Aoun, C. Frochot, M. Gary-Bobo, M. Kobeissi and F. Odobel, *Inorg. Chem.*, 2019, **58**, 12395-12406.
10. (a) R. F. Einrem, K. J. Gagnon, A. B. Alemayehu and A. Ghosh, *Chem.– Eur. J.*, 2016, **22**, 517-520. ;(b) R. F. Einrem, A. B. Alemayehu, S. M. Borisov, A. Ghosh and O. A. Gederaas, *ACS omega*, 2020, **5**, 10596-10601.;
11. (a) A. B. Alemayehu, K. J. Gagnon, J. Terner and A. Ghosh, *Angew. Chem., Int. Ed.*, 2014, **53**, 14411-14414.; (b)S. M. Borisov, A. Alemayehu and A. Ghosh, *J. Mater. Chem. C.*, 2016, **4**, 5822-5828.
12. (a) J. H. Palmer, A. C. Durrell, Z. Gross, J. R. Winkler and H. B. Gray, *J. Am. Chem. Soc*, 2010, **132**, 9230-9231.; (b) W. Sinha, L. Ravotto, P. Ceroni and S. Kar, *Dalton Trans.*, 2015, **44**, 17767-17773.; (c) I. K. Thomassen, L. J. McCormick-McPherson, S. M. Borisov and A. Ghosh, *Sci. Rep.*, 2020, **10**, 1-9.
13. A. B. Alemayehu, L. J. McCormick, K. J. Gagnon, S. M. Borisov and A. Ghosh, *ACS omega*, 2018, **3**, 9360-9368.
14. M. Toganoh, T. Niino and H. Furuta, *Chem. Commun.*, 2008, 4070-4072.
15. A. B. Alemayehu, N. U. Day, T. Mani, A. B. Rudine, K. E. Thomas, O. A. Gederaas, S. A. Vinogradov, C. C. Wamser and A. Ghosh, *ACS Appl. Mater. Interfaces*, 2016, **8**, 18935-18942.
16. C. M. Lemon, *Pure Appl. Chem.*, 2020, **92**, 1901-1919.
17. C. Di Natale, C. P. Gros and R. Paolesse, *Chem. Soc. Rev.***,** 2022, **51**, 1277-1335
18. X. Zhan, W. Lee, K. Sudhakar, D. Kim, A. Mahammed, D. G. Churchill and Z. Gross, *Inorg. Chem.*, 2021, **60**, 8442-8446.
19. A. B. Alemayehu and A. Ghosh, *J. Porphyrins Phthalocyanines*, 2011, **15**, 106-110.
20. E. Rabinovich, I. Goldberg and Z. Gross, *Chem. Eur. J.*, 2011, **17**, 12294-12301.
21. K. E. Thomas, A. B. Alemayehu, J. Conradie, C. Beavers and A. Ghosh, *Inorg. Chem.*, 2011, **50**, 12844-12851.
22. K. E. Thomas, C. M. Beavers and A. Ghosh, *Mol. Phys.*, 2012, **110**, 2439-2444.
23. S. L. Lai, L. Wang, C. Yang, M. Y. Chan, X. Guan, C. C. Kwok and C. M. Che, *Advanced Functional Materials*, 2014, **24**, 4655-4665.
24. R. D. Teo, H. B. Gray, P. Lim, J. Termini, E. Domeshek and Z. Gross, *Chem. Commun.*, 2014, **50**, 13789-13792.
25. W. Sinha, M. G. Sommer, M. van der Meer, S. Plebst, B. Sarkar and S. Kar, *Dalton Trans.*, 2016, **45**, 2914-2923.

26. J. Capar, J. Zonneveld, S. Berg, J. Isaksson, K. J. Gagnon, K. E. Thomas and A. Ghosh, *J. Inorg. Biochem*, 2016, **162**, 146-153.
27. M. Soll, K. Sudhakar, N. Fridman, A. Müller, B. Röder and Z. Gross, *Org. Lett.*, 2016, **18**, 5840-5843.
28. K. Sudhakar, A. Mizrahi, M. Kosa, N. Fridman, B. Tumanskii, M. Saphier and Z. Gross, *Angew. Chem., Int. Ed.*, 2017, **56**, 9837-9841.
29. C. M. Lemon, D. C. Powers, P. J. Brothers and D. G. Nocera, *Inorg. Chem.*, 2017, **56**, 10991-10997.
30. K. E. Thomas, K. J. Gagnon, L. J. McCormick and A. Ghosh, *J. Porphyrins Phthalocyanines*, 2018, **22**, 596-601.
31. R. F. Einrem, E. T. Jonsson, S. J. Teat, N. S. Settineri, A. B. Alemayehu and A. Ghosh, *RSC Adv.*, 2021, **11**, 34086-34094.
32. J. Terner, K. E. Thomas, H. Vazquez-Lima and A. Ghosh, *J. Inorg. Biochem.*, 2022, **231**, 111783.
33. (a) K. Sahu, S. Mondal, S. M. Mobin and S. Kar, *J. Org. Chem.* , 2021, **86**, 3324-3333.;(b) K. Sahu, J. Dutta, S. Nayak, P. Nayak, H. S. Biswal and S. Kar, *Inorg. Chem.*, 2022, **61**, 6539-6546.
34. R. W.-Y. Sun and C.-M. Che, *Coord. Chem. Rev.*, 2009, **253**, 1682-1691.
35. L. He, T. Chen, Y. You, H. Hu, W. Zheng, W. L. Kwong, T. Zou and C. M. Che, *Angew. Chem. Int. Ed.* , 2014, **126**, 12740-12744.
36. A. D. Lammer, M. E. Cook and J. L. Sessler, *J. Porphyr. Phthalocyanines*, 2015, **19**, 398-403.
37. H. Echizen, E. Sasaki and K. Hanaoka, *Biomolecules*, 2021, **11**, 1553.
38. H. Lim, K. E. Thomas, B. Hedman, K. O. Hodgson, A. Ghosh and E. I. Solomon, *Inorg. chem.*, 2019, **58**, 6722-6730.
39. S. Ganguly and A. Ghosh, *Acc. Chem. Res.*, 2019, **52**, 2003-2014.
40. C. Hansch, A. Leo and R. Taft, *Chem. rev.*, 1991, **91**, 165-195.
41. J. Conradie, C. C. Wamser and A. Ghosh, , *J. Phys. Chem. A*, 2021, **125**, 9953-9961.
42. A. Ghosh and J. Conradie, , *J. Phys. Chem. A*, 2021, **125**, 9962-9968.
43. A recent study [42] described Au[TPC] as a hypsocorrole, by analogy with hypsoporphyrins. The redshifts induced by thiocyanation, however, blurs the hypso/hyper distinction for Au[TPC(SCN)$_4$].
44. B. Koszarna and D. T. Gryko, *J. Org. Chem.* , 2006, **71**, 3707-3717.
45. G. A. Crosby and J. N. Demas, *J. Phys. Chem.*, 1971, **75**, 991-1024.
46. D. F. Eaton, *Pure Appl. Chem.*, 1988, **60**, 1107-1114.
47. F. Wilkinson, W. P. Helman and A. B. Ross, *J. Phys. Chem. Ref. Data* 1993, **22**, 113-262.
48. G. M. Sheldrick, *Acta Crystallogr. A*, 2008, **64**, 112-122.
49. P. Van der Sluis and A. Spek, *Acta Crystallogr., Sect. A: Found. Crystallogr.*, 1990, **46**, 194-201.
50. C. Lee, W. Yang and R. G. Parr, *Phys. Rev. B ,* 1988, **37**, 785.
51. N. C. Handy and A. J. Cohen, *Mol. Phys.* , 2001, **99**, 403-412.
52. A. Becke, *Chem. Phys*, **98**, 5648.
53. M. Reiher, O. Salomon and B. Artur Hess, *Theor. Chem. Account*, 2001, **107**, 48-55.
54. S. Grimme, J. Antony, S. Ehrlich and H. Krieg, *J. Chem. Phys.* , 2010, **132**, 154104.
55. A. Klamt and G. Schuurmann, *J.Chem.Soc.*,*Perkin Trans. 2*, 1993,799-805.
56. A. Klamt, *J. Phys. Chem.*, 1995, **99**, 2224-2235.
57. E. v. Lenthe, E.-J. Baerends and J. G. Snijders, *J. Chem. Phys.* , 1993, **99**, 4597-4610.
58. E. van Lenthe, E.-J. Baerends and J. G. Snijders, *J. Chem. Phys.* , 1994, **101**, 9783-9792.
59. E. Van Lenthe, A. Ehlers and E.-J. Baerends, *J. Chem. Phys.*, 1999, **110**, 8943-8953.
60. G. t. Te Velde, F. M. Bickelhaupt, E. J. Baerends, C. Fonseca Guerra, S. J. van Gisbergen, J. G. Snijders and T. Ziegler, *J. Comput. Chem.*, 2001, **22**, 931-967.
61. DFT has an extensive track record of reproducing ionization potentials and photoelectron spectra of porphyrin-type molecules.
62. A. Ghosh and J. Almlöf, *Chem. Phys. Lett.,* 1993, **213**, 519-521.
63. A. Ghosh, *J. Am. Chem. Soc.*, 1995, **117**, 4691–4699.

64. A. Ghosh, *J. Phys. Chem. B,* 1997, **101**, 3290-3297.
65. A. Ghosh and T. Vangberg, *Theor. Chem. Acc.* , 1997, **97**, 143-149.
66. A. Ghosh, *Acc. Chem. Res.* , 1998, **31**, 189-198.
67. Electron affinities of metalloporphyrin-type molecules have been less intensively studied, compared with ionization potentials. DFT calculations, however, are thought to provide an excellent description of metal- versus ligand-centered reduction for such systems.
68. H. Ryeng, E. Gonzalez and A. Ghosh, *J. Phys. Chem.B*, 2008, **112**, 15158-15173.
69. K. E. Thomas, H. Vazquez-Lima, Y. Fang, Y. Song, K. J. Gagnon, C. M. Beavers, K. M. Kadish and A. Ghosh, *Chem. Eur. J.*, 2015, **21**, 16839–16847.
70. J. Michl, *Pure Appl. Chem.*, 1980, **52**, 1549-1563.

Graphical abstract

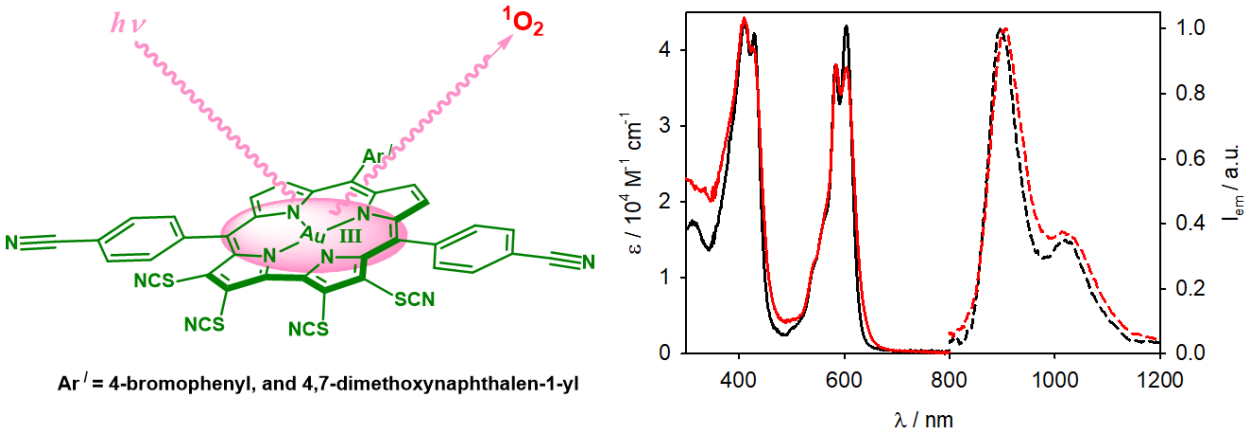

Tetra(thiocyano)corrolato-Au(III) derivatives showed phosphorescence at the near-infrared region (at ca. 900 nm) at ambient temperature with relatively long phosphorescent lifetimes of 10 μs. The phosphorescence appeared at a longer wavelength than the previously reported other gold(III) corroles/porphyrins. In addition, these compounds can efficiently sensitize singlet oxygen with singlet oxygen production quantum yields of ca. 50% efficiency in chloroform solution.